

AN EMPIRICAL FITTING METHOD FOR TYPE IA SUPERNOVA LIGHT CURVES. II. ESTIMATING THE FIRST-LIGHT TIME AND RISE TIME

WEIKANG ZHENG^{1,2}, PATRICK L. KELLY¹, AND ALEXEI V. FILIPPENKO^{1,3}

Draft version March 11, 2022

ABSTRACT

We investigate a new empirical fitting method for the optical light curves of Type Ia supernovae (SNe Ia) that is able to estimate the first-light time of SNe Ia, even when they are not discovered extremely early. With an improved ability to estimate the time of first light for SNe Ia, we compute the rise times for a sample of 56 well-observed SNe Ia. We find rise times ranging from 10.5 to 20.5 days, with a mean of 16.0 days, and confirm that the rise time is generally correlated with the decline rate $\Delta m_{15}(B)$, but with large scatter. The rise time could be an additional parameter to help classify SN Ia subtypes.

Subject headings: methods: data analysis — supernovae: general

1. INTRODUCTION

Type Ia supernovae (SNe Ia) are believed to be thermonuclear runaway explosions of carbon/oxygen white dwarfs (see, e.g., Hillebrandt & Niemeyer 2000 for a review). The relationship between the light-curve decline and the peak brightness, known as the “Phillips relation” (Phillips 1993; Phillips et al. 1999), makes SNe Ia excellent calibratable candles, most notably leading to the discovery of the accelerating expansion of the Universe (Riess et al. 1998; Perlmutter et al. 1999).

While much effort has been focused on the post-maximum part of SN Ia light curves and an important parameter $\Delta m_{15}(B)$ (e.g., Phillips 1993; Phillips et al. 1999), there are few studies of the pre-maximum rise, in part because very few SNe Ia were discovered at extremely early times — hence, it was difficult to derive accurate rise times. But the number of known very young SNe Ia has increased in the past few years, making it possible to measure their initial behaviour and estimate their first-light time.⁴ Riess et al. (1999) used 30 early-time unfiltered CCD observations of SNe Ia and adopted the commonly known t^2 function (from the expanding fireball model; see, e.g., Arnett 1982; Riess et al. 1999; Arnett et al. 2016) to measure the rise time, finding $t_r = 19.5 \pm 0.2$ days. Conley et al. (2006) used a larger sample, 73 SNe Ia from the Supernova Legacy Survey and also adopted a t^2 function, deriving a similar rise time of 19.34 days. Hayden et al. (2010) used a “2-stretch” fit algorithm which estimates the rise and fall times independently, determining a shorter rise time of 17.38 ± 0.17 for a set of 391 SNe Ia from the Sloan Digital Sky Survey-II. This was followed by Ganeshalingam et al. (2011), who used a similar two-stretch template-fitting method and found that SNe Ia with high-velocity spectral features have a shorter rise time ($t_r = 16.63 \pm 0.29$

days) than normal SNe Ia ($t_r = 18.03 \pm 0.24$ days).

Ganeshalingam et al. (2011) also showed that the initial rise of a SN Ia light curve follows a power law (t^n) with index $n = 2.20$. Nugent et al. (2011) found a rising index of 2.01 for the light curve of SN 2011fe, very consistent with the commonly known t^2 function, and they use this to estimate the object’s first-light time. More SNe Ia were subsequently discovered at extremely early times, and thus the first-light time could be derived typically from the power law (t^n) function — e.g., SN 2012cg (Silverman et al. 2012b), SN 2013dy (Zheng et al. 2013), iPTF13ebh (Hsiao et al. 2015), ASASSN-14lp (Shappee et al. 2015), and the *Kepler* objects KSN 2012a, KSN 2011b, and KSN 2011c (Olling et al. 2015). Firth et al. (2015) adopted a more general t^n model to study a sample of 18 SNe Ia and found a mean uncorrected rise time of 18.98 days, with $n = 1.5$ to > 3.0 and a mean value of 2.44.

In this paper, we apply an empirical fitting method proposed by Zheng & Filippenko (2017) to a large sample of SNe Ia with well-observed optical light curves and thereby estimate the explosion time t_0 . Once t_0 is derived, the rise time t_r is easily determined as long as the time of peak brightness, t_p , is also measured. Note that the quantity we determine from the data is actually the first-light time (t_{0f}) rather than the true explosion time (t_0). However, here we do not distinguish between the two values; namely, we assume $t_{0f} \approx t_0$, and use t_0 as the first-light time throughout the paper.

2. ANALYSIS

2.1. Fitting Method

Zheng & Filippenko (2017) proposed an empirical function that can well fit the optical light curves of SNe Ia. It is a variant of the broken-power-law function shown as

$$L = A' \left(\frac{t - t_0}{t_b} \right)^{\alpha_r} \left[1 + \left(\frac{t - t_0}{t_b} \right)^{s\alpha_d} \right]^{-2/s}, \quad (1)$$

where A' is a scaling constant, t_0 is the first-light time, t_b is the break time, α_r and α_d are the two power-law indices before and after the break (respectively), and s is a transition parameter. This function⁵ is mathematically

⁵ Note that Equation 1 is mathematically very similar to the generalised Pareto distribution in statistics (e.g., Abd Elfattab et

¹ Department of Astronomy, University of California, Berkeley, CA 94720-3411, USA

² e-mail: zwk@astro.berkeley.edu

³ Senior Miller Fellow, Miller Institute for Basic Research in Science, University of California, Berkeley, CA 94720, USA

⁴ SNe Ia may experience a “dark phase” (which could last for a few hours to days) between the moment of explosion and the first observed light (e.g., Rabinak et al. 2012; Piro & Nakar 2013, 2014).

analytic, derived directly from the photospheric velocity evolution function with some reasonable assumptions. Zheng & Filippenko (2017) show that this function can well fit the optical light curves of the prototypical Type Ia SN 2011fe, where they fixed t_0 during the fitting process because it is well estimated (see Nugent et al. 2011). In the following section, we expand this method to a set of nine extremely well-observed SNe Ia, estimating their values of t_0 (which means we treat t_0 as a free parameter during the fitting). We then apply the method to a larger sample of SNe Ia having well-observed optical light curves.

2.2. Fitting to the Extremely Good Sample

We adopt an IDL implementation of *mpfit* (Markwardt 2009)⁶ for all the fitting procedures. During our test fitting, we found that it is difficult to well constrain t_0 if t_0 , α_r , and s are all set free, because these three parameters are related when estimating t_0 . Hence, it is necessary to fix a few other parameters in order to get a good constraint on t_0 . But before doing that, it is important to understand each parameter and statistically study them with at least a few SNe Ia.

Fortunately, there are nine SNe Ia that were discovered very early and monitored well thereafter, making them suitable for our purposes. Their first-light times are well estimated directly from the data; thus, for these SNe Ia, we could fix t_0 during the fitting and then study the properties of the other parameters in Equation 1. This well-observed SN Ia sample (see Table 1) includes SN 2009ig (Foley et al. 2009), SN 2011fe (Nugent et al. 2011), SN 2012cg (Silverman et al. 2012b), SN 2013dy (Zheng et al. 2013), iPTF13ebh (Hsiao et al. 2015), ASASSN-14lp (Shappee et al. 2015), and three SNe Ia discovered by the *Kepler* spacecraft (KSN 2012a, KSN 2011b, and KSN 2011c; Olling et al. 2015). Most of them are normal SNe Ia, except for the three *Kepler* SNe with unknown subtype since we only have broadband light curves but no spectra, and iPTF13ebh which was categorized as a “transitional” event between normal SNe Ia and the fast-declining subluminous SN 1991bg-like objects owing to its relative largely $\Delta m_{15}(B)$ (1.79; see Hsiao et al. 2015).

We first fit the light curves by fixing t_0 because it is already well estimated for each SN. We then apply the fitting independently to each filter, including the data points from the beginning of the observational campaign until the SN entered the phase dominated by cobalt decay, which usually happens around three weeks after peak brightness in the *B* and *V* bands.

Since SNe Ia generally exhibit a shoulder in the *R* band and a second peak in the *I* band, we restrict the fits to earlier times in the redder bands (*R*, *I*) than in the bluer bands (*B*, *V*). Specifically, for the *R* and *I* bands, the data points are cut off before the shoulder appears, but still after the main peak. For a few cases, additional *U*-band data or *g*, *r*, or *i* filters were used. Data with all of these filters are treated independently. Additionally, the three *Kepler* SNe were observed with a broad filter that

al. 2007; Raja & Mir 2013). It is unclear whether there is any physical connection between the light-curve shape and the generalised Pareto distribution; further studies are needed to further elucidate possible associations.

⁶ <https://www.physics.wisc.edu/~craigm/idl/fitting.html>

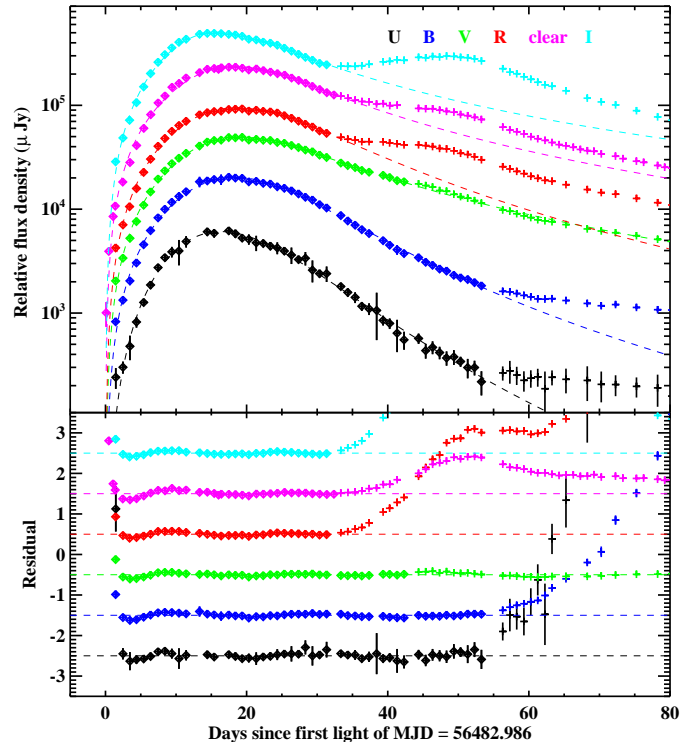


FIG. 1.— Multiband light-curve fitting of SN 2013dy using Equation 1, arbitrarily shifted for clarity. The value of t_0 is fixed to be t_{0f} (MJD 56482.986) during the fitting. Diamond-shaped data points are included in the fitting while cross-shaped ones are excluded.

is quite different from any existing standard filter. However, since we fit all filtered data independently, we apply the same fitting to the three *Kepler* SNe. Only when plotting, we represent these objects with the *R* band, since the *Kepler* response function covers the wavelength range 420–900 nm and peaks around 600 nm (see the *Kepler* website⁷).

The fitting procedure is very similar for each SN as well as for each filter; thus, we show only one case as an example. Figure 1 illustrates the fitting results for SN 2013dy, with comments similar to those for the fitting of SN 2011fe by Zheng & Filippenko (2017; see their Figure 2).

As shown in Figure 1, by using just one single function given by Equation 1, the fitting results are surprisingly good for the included data, which cover a long time range and nearly a factor of 100 in flux (~ 5 mag) for all filters (*U*, *B*, *V*, *R*, *clear*, and *I*). In particular, for the *V* band, although we include only the data up to day 45, the model still matches the data well up to nearly three months after the explosion (though this might be just a coincidence). The flux residuals are mostly within the 1σ measurement uncertainties.

Using the same procedure, we apply the fitting to the eight other well-observed SNe Ia by fixing t_0 . In general, the fitting results are very similar to those of SN 2013dy shown in Figure 1, though they do show some indication for diversity at extremely early times. For a few cases in our sample including SN 2012cg and SN 2013dy, we find for the first few days (within three days after first-light

time) that the data show an excess compared to the fit model, possibly from other contributions such as thermal emission produced by the impact of the SN shock on a binary companion star (e.g., Kasen 2010; Cao et al. 2015; Marion et al. 2016). In principle, for our purposes it is more appropriate to exclude these data from the fitting; we therefore excluded data within 3.0 days after t_0 during the fitting. However, in our later analysis of the first-light time estimation (in Section 2.3), we find that this early-time excess insignificantly affects the estimate (the changes are much smaller than the fitting error itself), so in Section 2.3 we retain these data during the fitting process.

After fitting to all 9 of the SNe given above, we plot the histogram distribution in Figure 2 for each parameter from Equation 1, including t_b , α_r , α_d , and s , but not t_0 (which was fixed during the fitting procedure) and A' (which is simply a scaling factor). Note that since some SNe lack observations in one or a few filters, not all filters have the complete set of 9 data points representing 9 SNe; however, whichever filter was observed is fitted independently and shown in the figure. These fitting results are also listed in Table 1.

As shown in Figure 2, it is clear that α_r (top-right panel) is the most concentrated parameter, with a mean value of 1.90 ± 0.18 - very consistent with the commonly known t^2 model for most SNe Ia or the t^n model (n varies from ~ 1.5 to ~ 3.0) studied by various groups (e.g., Conley et al. 2006; Ganeshalingam et al. 2011; Firth et al. 2015). The parameter with the next-smallest dispersion is the break time t_b (top-left panel), with a mean value of 23.0 ± 4.0 days, typically a few days after the time of peak brightness. The other two parameters, s (the smoothing parameter) and α_d , are much less concentrated.

In conclusion, to better estimate the first-light time t_0 (as shown in the next section), it is appropriate to keep α_r and t_b constant during the fitting procedure because for each filter these two parameters exhibit a small dispersion among different SNe. Conversely, it is best to keep s and α_d as free parameters, since they are quite diverse. By doing this, Equation 1 has fewer free parameters (only 4, after fixing α_r and t_b), and we can better constrain t_0 as demonstrated below.

2.3. Estimating t_0 with the Extremely Good Sample

In reality, very few SNe Ia have been discovered extremely early like the nine SNe mentioned above. However, for SNe Ia that were discovered reasonably early (1–2 weeks after explosion), one may estimate the explosion time t_0 by fitting the light curve using Equation 1.

Before applying this method to a larger set we need to test its validity. Our set of 9 well-observed SNe Ia provides a perfect sample for such test, since all of them already have a well-determined t_0 (which we denote as “known t_0 ”). We can then compare the “known t_0 and the t_0 value estimated from fitting Equation 1 to study the errors from the fitting method.

First, in order to simulate the relatively late-time discovery for the majority of less well-observed SNe Ia, we intentionally exclude some of the very early-time data points for the above 9 SNe. However, a criterion needs to be established for how late to start using the data. Here we define the limit to be the time prior to peak brightness when the SN is 1 mag fainter than the peak magnitude,

denoted by $t_{\text{pm}-1}-0$; it typically occurs around 1–2 weeks before peak brightness. The first data point must be at least 1 mag fainter than the peak magnitude. We adopt this limit for selecting SNe to be fitted with Equation 1 because we require relatively early-time observations to constrain t_0 . If there are additional observations one day earlier than that, their time will be denoted by $t_{\text{pm}-1}-1$, and so on. The discovery times of the above 9 SNe are extremely early, in some cases reaching $t_{\text{pm}-1}-7$.

Next, in order to simulate the different discovery times of most SNe, for each of the above 9 well-observed SNe we gradually include data points earlier than $t_{\text{pm}-1}-0$ until all data are included. Each step gives a corresponding $t_{\text{pm}-1}X$ value (X varies from 0 to -7). We then use Equation 1 to fit t_0 , and we compare the estimated value with the “known t_0 .” Again, we use SN 2013dy as an example to demonstrate this procedure, which is very similar for all of our 9 SNe in each band. Figure 3 illustrates the case of SN 2013dy with $t_{\text{pm}-1}-3$. Note the difference with Figure 1; now we include only data after $t_{\text{pm}-1}-3$ in order to simulate a late discovery. The data before $t_{\text{pm}-1}-3$ are shown as crosses, which means they are not included. As mentioned above, for all fitting to estimate t_0 , we fix α_r to be 1.90 and t_b to be 23.0.

After applying the t_0 fit to each SN for each band, and for each case with different $t_{\text{pm}-1}X$ (X varies from 0 to -7), we compare the estimated t_0 with the “known t_0 .” The result is shown in Figure 4, where the upper panel shows the cases for each SN and each filter with different $t_{\text{pm}-1}X$. For a certain $t_{\text{pm}-1}X$, if there is more than one filter observed for a SN (as shown in Table 1, except for the three *Kepler* SNe that were only observed with one broadband filter), a mean value of t_0 from all filters is also calculated. The bottom panel shows the histogram of the t_0 offsets compared with the “known t_0 ”; each filter is color coded.

Three important and clear conclusions can be drawn from Figure 4. First, the offset between the fitting t_0 and the “known t_0 ” becomes smaller when earlier data are included — namely, the smaller the X value in $t_{\text{pm}-1}X$, the smaller the offset. But once X reaches -3 , then even earlier data do not help much for t_0 estimation. Second, B interestingly has the smallest offset, and no matter when starting with $t_{\text{pm}-1}X$, the offset is always within ± 1.5 days; we estimate a 1σ systematic error of ± 0.7 days by adopting only the B -band estimate of the t_0 offset. Third, the mean offset with multiple filters is similar to that of the B band; thus, for t_0 estimation, one should use either the mean value or the value estimated from B alone. Technically, it is not surprising to see why the B band gives the best estimate of t_0 ; in other bands, the peak is usually broader than that of B , making B better for estimating t_0 . Because of this, in the following we only adopt the t_0 estimate from B , even if the SN was observed with multiple filters. We will also add a systematic error of ± 0.7 days for the t_0 estimated from B -band fitting.

In addition, Figure 4 shows that the fixed value of $\alpha_r = 1.90$ is appropriate, giving a mean t_0 offset of 0.1 ± 0.7 days for the B band, very close to 0 as expected. We further performed two other sets of fitting with the α_r value fixed to be 1.50 and 2.30 (respectively), and found t_0 offset by 1.2 ± 0.8 and -0.8 ± 0.7 for B , confirming that the fixed value of $\alpha_r = 1.90$ is appropriate.

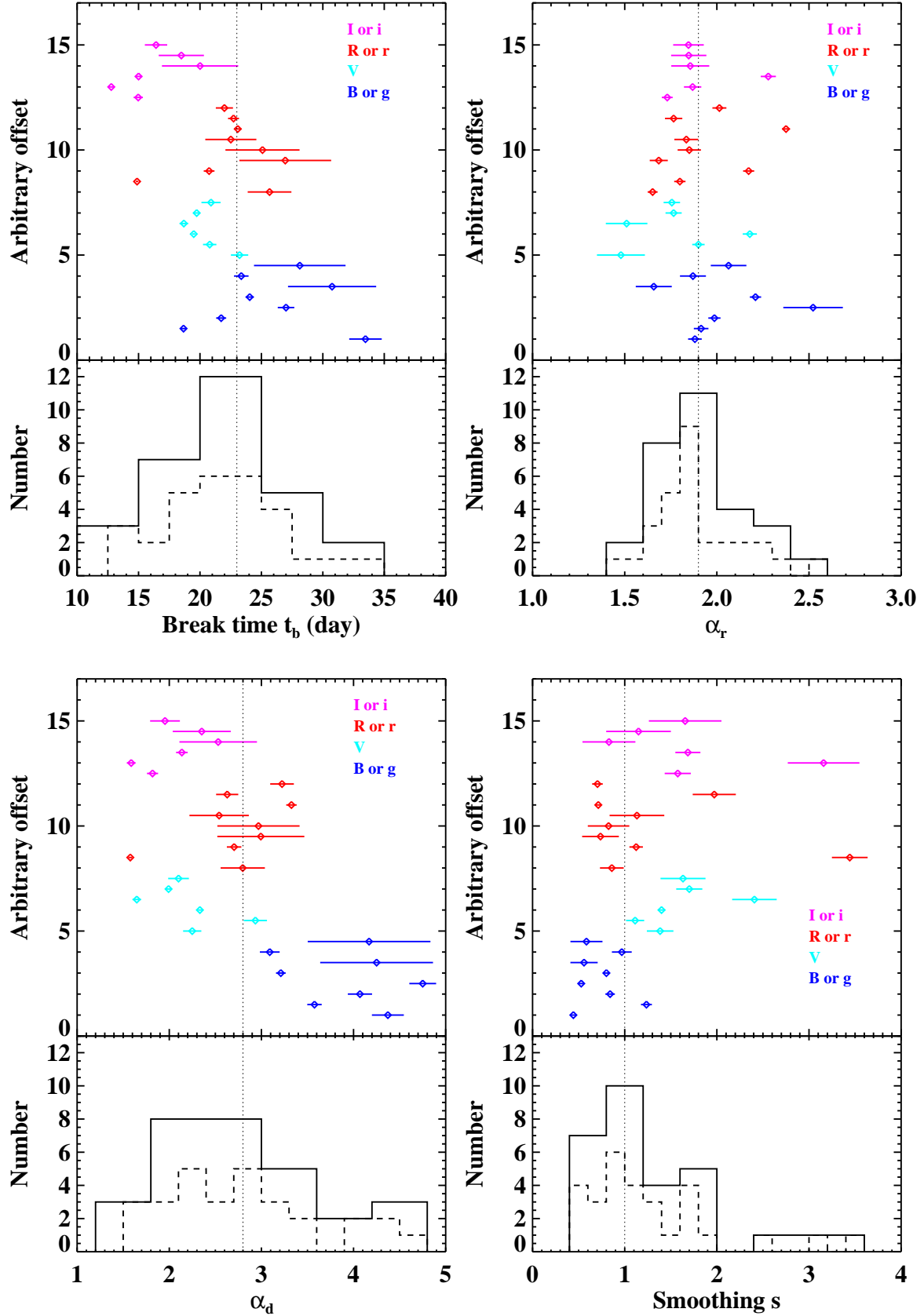


FIG. 2.— Individual points and histogram distribution of each fit parameter from Equation 1, including t_b (top left), α_r (top right), α_d (bottom left), and s (bottom right). For each parameter, the upper panel shows the individual value from different filters and the lower panel displays the histogram distribution with two different bin sizes.

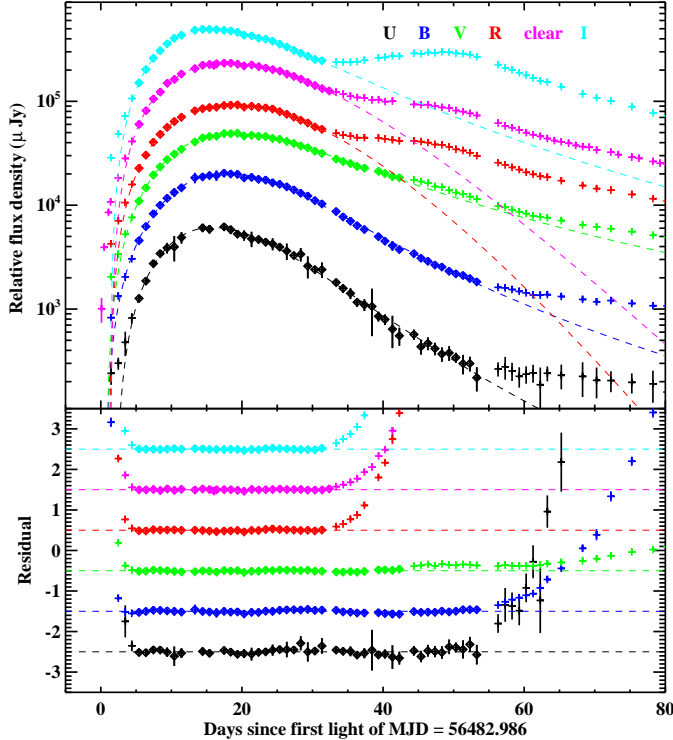


FIG. 3.— Multiband light-curve fitting of SN 2013dy using Equation 1 for estimating t_0 . The value of α_r is fixed to be 1.90 and t_b is fixed to be 23.0 during the fitting procedure. Diamond-shaped data points are included in the fitting while cross-shaped ones are excluded.

2.4. A Larger Well-Observed Sample for t_0 Estimation

From the above analysis, we have shown that Equation 1 provides a practical way to estimate t_0 by fixing α_r (to be 1.90) and t_b (to be 23.0) during fitting, and using only B (or g) data. Such an estimate of t_0 gives an additional systematic error of ± 0.7 days. We can now apply this method to a larger sample of objects that were typically discovered around $t_{\text{pm}-1} - 0$, or slightly earlier, but still with good-coverage observations after discovery.

Ganeshalingam et al. (2010) published a sample of 165 SNe Ia from the Lick Observatory Supernova Search (LOSS; Filippenko et al. 2001; Leaman et al. 2011) database. From this sample, we selected 44 SNe Ia that are suitable for our purpose. As above, all satisfy the criterion that the first observation is earlier than the time that the SN brightness reaches one magnitude fainter than the peak ($t_{\text{pm}-1} - 0$). (Of course, even earlier observations are preferred.) This lower limit criterion allowed us to choose 44 of the 165 LOSS SNe Ia. In addition, 6 SNe Ia were selected from the Harvard-Smithsonian Center for Astrophysics Data Release 3 (CfA3; Hicken et al. 2009), as well as 6 SNe Ia from the Carnegie Supernova Project (CSP; Contreras et al. 2010), making the final sample 56 SNe Ia, as listed in Table 2.

2.5. Rise-Time Estimation

We applied the fitting to the above 56 SNe Ia using Equation 1 only with B data (no g -band data were collected for these 56 SNe Ia), and fixing α_r to be 1.90 and t_b to be 23.0. The resulting t_0 estimates are listed in Table 2.

Once the first-light time t_0 is estimated, it is easy to

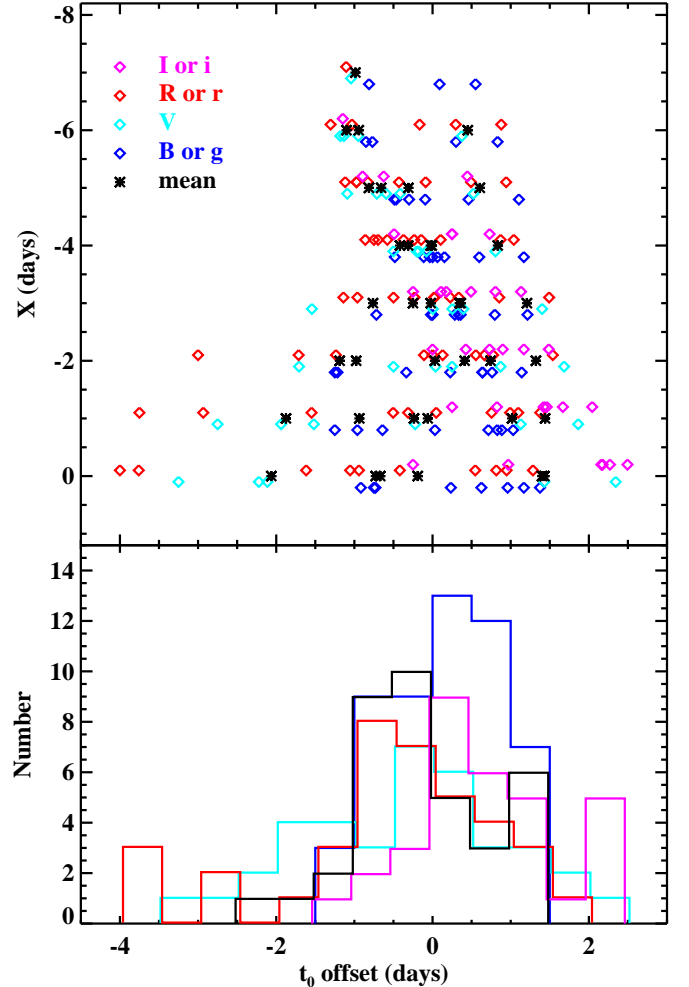


FIG. 4.— Difference of first-light time t_0 estimated from Equation 1 fitting with the real t_0 . Upper panel shows the cases for each SN and each filter with different $t_{\text{pm}-1}X$, arbitrarily shifted along the ordinate for clarity. The bottom panel shows the histogram of t_0 offsets for each filter, also arbitrarily shifted along the abscissa for clarity. In general, the smaller the X in $t_{\text{pm}-1}X$ (with earlier data), the smaller the offset. The B (or g) band has the smallest offset, and appears to not change with X , with a 1σ systematic error of ± 0.7 days.

calculate the rise time as long as the time of peak brightness can also be determined. Technically, it is much easier to estimate the peak time than the first-light time t_0 . Although the above fitting method can also give the peak time, it is more accurate and straightforward to estimate the peak time directly by fitting the light curve around peak brightness with a low-order polynomial. The time of peak B -band brightness is given in Table 2, along with the decline rate $\Delta m_{15}(B)$. The rise time is simply the time duration from first-light time to the time of peak brightness, corrected for time dilation through division by $1+z$; see Table 2 for the final results.

3. DISCUSSION

Unlike traditional light-curve fitting, which usually compares with templates, our estimation of the first-light time t_0 and rise time t_r are model independent; they are direct measurements of the observed data.

Figure 5 shows the histogram (left) and the cumulative (right panel) distribution of t_r of the 56 SNe Ia in our

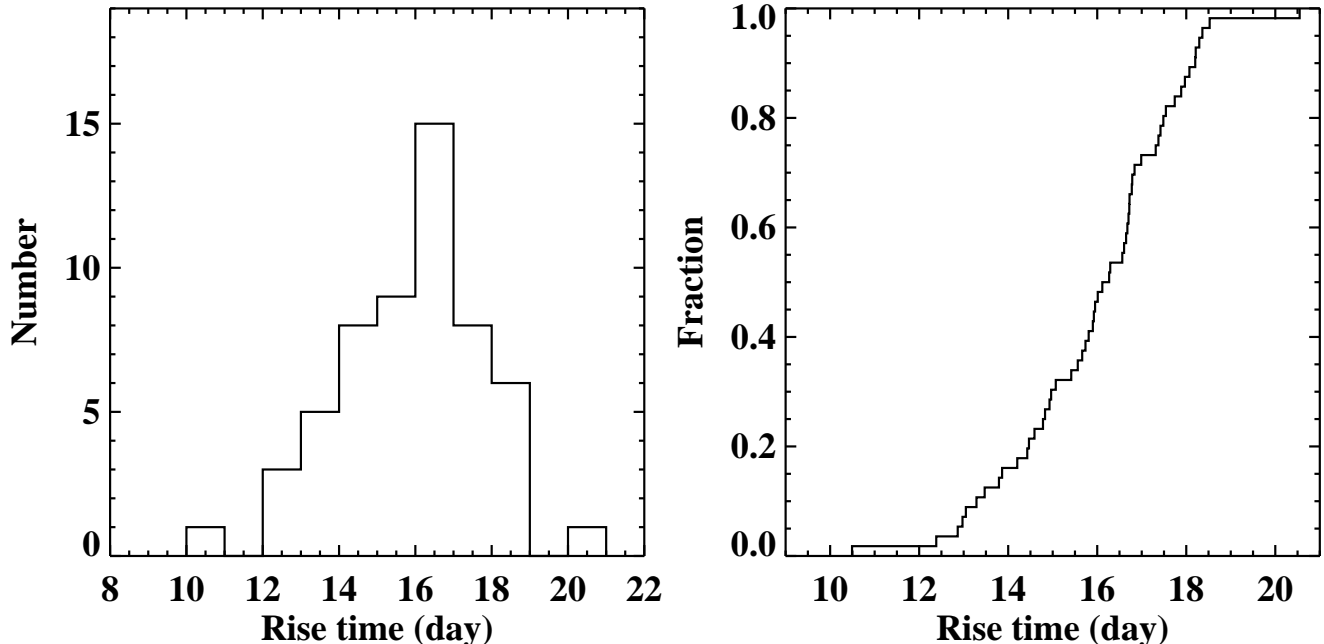


FIG. 5.— Histogram (left panel) and cumulative (right panel) distribution of rise times t_r from the 56 SNe Ia in our sample. The mean rise time is 16.0 days.

sample. The rise time varies from 10.5 days to 20.5 days with quite a wide range and concentrated around 16.0 days. The shortest rise time (10.5 days) is for SN 2003Y, a SN 1991bg-like (e.g., Filippenko et al. 1992a) sub-luminous SN Ia, while the longest (20.5 days) is for SN 2005M, a SN 1991T-like (e.g., Filippenko et al. 1992b) overluminous SN Ia. The remaining SNe have rise times between 12.0 and 19.0 days, with a mean value of 16.0 days, slightly longer than two weeks. Note that our estimate is slightly shorter than the mean rise time of 18.98 days derived by Firth et al. (2015), probably because their fitting model differs from ours.

In Figure 6, we compare the rise time t_r with two other important parameters for SNe Ia. At left, we plot t_r as a function of decline rate $\Delta m_{15}(B)$. There is an apparent correlation between the two parameters: the larger the rise time, the smaller the decline rate, and our best fit gives $t_r = -4.0 \times \Delta m_{15}(B) + 20.7$. However, this relation has a 1σ scatter of 1.3 days, estimated from the residuals of the whole sample, as shown in the bottom-left panel of Figure 6. This large scatter indicates that a single decline-rate parameter might not be enough to characterize the SN Ia light curve. In the right-hand panel, we plot t_r as a function of Δ from MLCS2k2 fitting (Jha et al. 2007), known as the stretch parameter. There is also a clear correlation: larger rise times have smaller values of Δ , and our best fit gives $t_r = -3.2 \times \Delta + 16.4$. This relation is substantially tighter than the previous one, with a 1σ scatter of only 1.0 days.

It is not surprising that the scatter between the rise time with Δ is smaller than that with $\Delta m_{15}(B)$, because the stretch parameter Δ considers both the rising and declining portions of the light curve in the MLCS2k2 fitting (Jha et al. 2007). Our result confirms the Hayden et al. (2010) and Ganeshalingam et al. (2010) conclusion that a single parameter is not enough to characterise the light curve. However, here we focus on studying the rising part of the light curve, at which time the emission

from a SN Ia better approximates a blackbody as was assumed for deriving the fitting function Equation 1; the SN is optically thicker at early times than during the decay. Although the rising and decaying parts are correlated, our results indicate that the scatter is large, so for some purposes it is better to distinguish the two sections.

Interestingly, but not surprisingly, most of the short-rise-time objects are sub-luminous SNe Ia (similar to the subtype of SN 1991bg-like SNe Ia), while those with longer rise times are overluminous SNe Ia (similar to the subtype of SN 1991T-like and SN 1999aa-like SNe Ia, see Li et al. (2001)).

In our sample, among the six objects with $t_r < 13.5$ days, three [SN 2003Y (Matheson et al. 2003), SN 2005ke (Patat et al. 2005), and SN 1999by (Howell et al. 2001)] are spectroscopically classified as SN 1991bg-like. SN 2002dl is also spectroscopically similar (Matheson et al. 2002) to the SN 1991bg-like SN 1999by. For one object (SN 2000dr), a spectrum from the UC Berkeley Supernova Database (UCB SNDB; Silverman et al. 2012a)⁸, shows that it best matches several normal SNe Ia about one week after maximum brightness based on the SN Identification code (SNID; Blondin & Tonry 2007), but it also matches the SN 1991bg-like SN 2007ba at +5 days; thus, SN 2000dr is also a possible SN 1991bg-like object. Spectra from UCB SNDB show that the final object (SN 2007ci) is likely a normal SN Ia. According to the five possible SN 1991bg-like SNe (including SN 2000dr), a good criterion for distinguishing SN 1991bg-like objects is $t_r < 13.5$ days if only using the rise time, but with one exception: SN 2007ci has a rise time of 13.0 days but is a normal SN Ia.

Similarly, among the 8 objects with $t_r > 18.0$ days, five of them [SN 1999dq (Jha et al. 1999), SN 2003fa (see spectra from the UCB SNDB), SN 2005M (Thomas

⁸ The SNDB was updated in 2015 and is available online at <http://heracles.astro.berkeley.edu/sndb/>

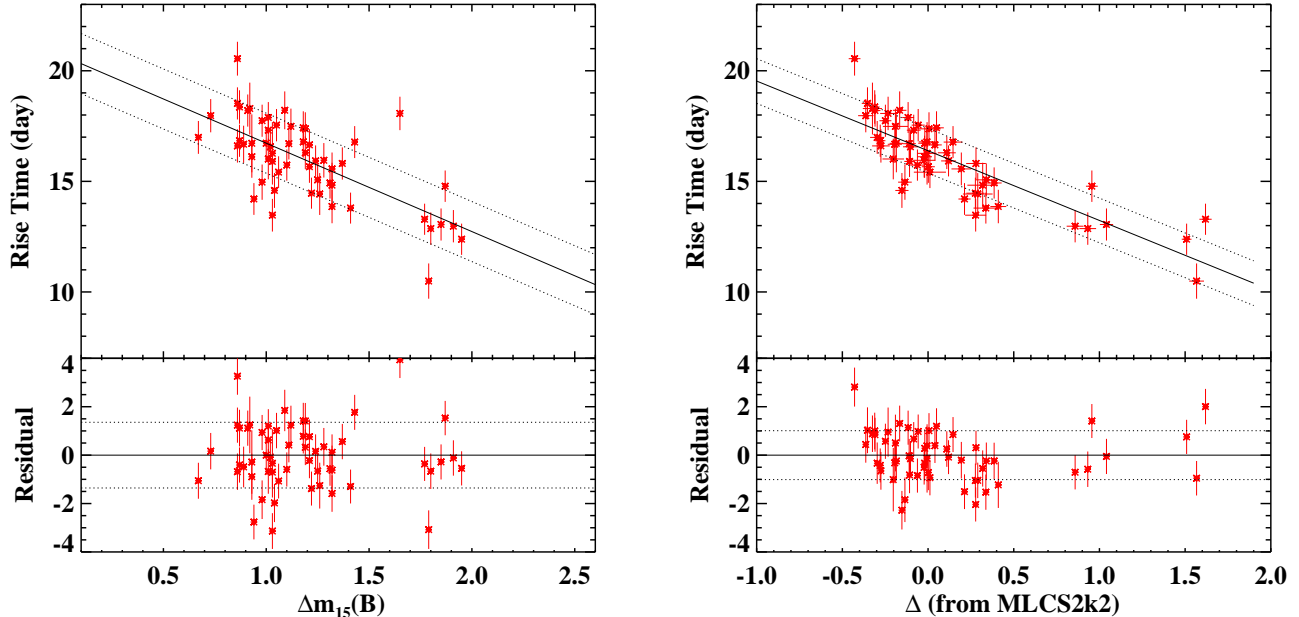


FIG. 6.— Rise time t_r as a function of decline rate $\Delta m_{15}(B)$ (left panel) and Δ from MLCS2k2 fitting (right panel), with a smaller scatter for the latter one. The bottom panels show the residuals from the best-fit relation. Dotted lines mark the 1σ scatter.

2005), SN 1999gp (Jha & Berlind 2000), and SN 2002eb (see spectra from UCB the SNDB)] are classified as SN 1991T-like or SN 1999aa-like objects. One of them (SN 2005hk) belongs to the SN Iax subclass (McCully et al. 2014). The other two [SN 2006ax (see spectra from Blondin et al. 2012) and SN 2006gr (see spectra from the UCB SNDB)] best match several normal SNe Ia but also a few SN 1999aa-like SNe; thus, SN 2006ax and SN 2006gr are also possibly SN 1999aa-like objects. According to the seven possible SN 1991T-like or SN 1999aa-like SNe (including SN 2006ax and SN 2006gr), a good criterion for distinguishing SN 1991T-like and SN 1999aa-like objects is $t_r > 18.0$ days if only using the rise time, but with one exception: SN 2005hk has a rise time of 18.1 days but is a SN Iax.

The above analysis shows that the rise time is an additional parameter helpful for classifying SN Ia subtypes.

4. CONCLUSIONS

We have adopted an empirical method to fit the optical light curves of SNe Ia which is useful for estimating their first-light time and rise time. Our method differs from the usual template-fitting method for SN Ia light curves; we give direct measurements of the first-light time and

rise time. From a sample of 56 well-observed SNe Ia, we find that the rise time ranges from 10.5 days to 20.5 days, with a mean rise time of 16.0 days. Our results confirm that the rise time is generally correlated with the decline rate $\Delta m_{15}(B)$ and stretch parameter Δ , but with large scatter, especially when using $\Delta m_{15}(B)$. We also show that the rise time is useful for SN Ia subtype classification.

We thank Isaac Shivvers and Melissa L. Graham for useful discussions and suggestions, as well as the staffs of the observatories where data were obtained. We also thank Brad E. Tucker for providing data for the three *Kepler* SNe Ia published by Olling et al. (2015). A.V.F.'s supernova group at UC Berkeley is grateful for financial assistance from NSF grant AST-1211916, the TABASGO Foundation, the Christopher R. Redlich Fund, and the Miller Institute for Basic Research in Science (U.C. Berkeley). The work of A.V.F. was completed in part at the Aspen Center for Physics, which is supported by NSF grant PHY-1607611; he thanks the Center for its hospitality during the neutron stars workshop in June and July 2017.

REFERENCES

- Abd Elfattah, A. M., Elsherpieny, E. A., & Hussein, E. A., 2007, *Interstat*, 12, 1
- Arnett, W. D. 1982, *ApJ*, 253, 785
- Arnett, W. D., Fryer, C. L., & Matheson, T. 2016, submitted (arXiv:1611.08746)
- Blondin, S., & Tonry, J. L. 2007, *ApJ*, 666, 1024
- Cao, Y., Kulkarni, S. R., Howell, D. A., et al., 2015, *Nature*, 521, 328
- Conley, A., Howell, D. A., Howes, A., et al., 2006, *ApJ*, 132, 1707
- Contreras, C., Hamuy, M., Phillips, M. M., et al., 2010, *ApJ*, 139, 519
- Filippenko A. V., Li W. D., Treffers R. R., Modjaz, M., 2001, in *Small-Telescope Astronomy on Global Scales.*, ed. B. Paczyński, W. P. Chen, & C. Lemme (San Francisco: ASP), 121
- Filippenko, A. V., Richmond, M. W., Branch, D., et al., 1992a, *AJ*, 104, 1543
- Filippenko, A. V., Richmond, M. W., Matheson, T., et al., 1992b, *ApJL*, 384, L15
- Firth, R. E., Sullivan, M., Gal-Yam, A., et al., 2015, *MNRAS*, 446, 3895
- Foley, R. J., Challis, P. J., Filippenko, A. V., et al., 2012, *ApJ*, 744, 38
- Ganeshalingam, M., Li, W., Filippenko, A. V., et al., 2010, *ApJS*, 190, 418

- Ganeshalingam, M., Li, W., Filippenko, A. V., 2011, MNRAS, 416, 2607
- Hayden, B. T., Garnavich, P. M., Kessler, R., et al., 2010, ApJ, 712, 350
- Hicken, M., Challis, P., Jha, S., et al., 2009, ApJ, 700, 331
- Hillebrandt, W., & Niemeyer, J. C., 2000, ARA&A, 38, 191
- Howell, D. A., Höflich, P., Wang, L., & Wheeler, J. C., 2001, ApJ, 556, 302
- Hsiao, E. Y., Burns, C. R., Contreras, C., et al., 2015, A&A, 578, 9
- Jha, S., & Berlind, P., 2000, IAU Circ., 7341
- Jha, S., Garnavich, P., Challis, P., Kirshner, R. P., & Berlind, P., 1999, IAU Circ., 7250
- Jha, S., Riess, A. G., & Kirshner, R., 2007, ApJ, 659, 122
- Kasen, D., 2010, ApJ, 708, 1025
- Leaman, J., Li, W., Chornock, R., & Filippenko, A. V., 2011, MNRAS, 412, 1419
- Li, W., Filippenko, A. V., Treffers, R. R., Riess, A. G., Hu, J., & Qiu, Y. 2001, ApJ, 546, 734
- Maguire, K., Sullivan, M., Thomas, R. C., et al., 2011, MNRAS, 418, 747
- Marion, G. H., Brown, P. J., Vinkó, J., et al., 2016, ApJ, 820, 92
- Matheson, T., Challis, P., Kirshner, R. P., Calkins, M., 2003, IAU Circ., 8063
- Matheson, T., Jha, S., Challis, P., Kirshner, R. P., & Berlind, P., 2002, IAU Circ., 7923
- McCully, C., Jha, S. W., Foley, R. J., et al., 2014, ApJ, 786, 134
- Nugent, P. E., Sullivan, M., Cenko, S. B., et al., 2011, Nature, 480, 344
- Olling, R. P., Mushotzky, R., Shaya, E., et al., 2015, Nature, 521, 332
- Patat, F., Baade, D., Wang, L., Taubenberger, S., & Wheeler, J. C., 2005, IAU Circ., 8631
- Perlmutter, S., Aldering, G., Goldhaber, G., et al., 1999, ApJ, 517, 565
- Piro, A., & Nakar, E. 2013, ApJ, 769, 67
- Piro, A., & Nakar, E. 2014, ApJ, 784, 85
- Rabinak, I., Livne, E., & Waxman, E. 2012, ApJ, 757
- Raja, R. A., & Mir, A. H., 2013, GJHSS, 13, 9
- Riess, A. G., Filippenko, A. V., Challis, P., et al., 1998, AJ, 116, 1009
- Shappee, B. J., Piro, A. L., Holoiu, T. W., et al., 2016, ApJ, 826, 144
- Silverman, J. M., Foley, R. J., Filippenko, A. V., et al. 2012a, MNRAS, 425, 1789
- Silverman, J. M., Ganeshalingam, M., Cenko, S. B., et al., 2012b, ApJ, 756, L7
- Thomas, R. C., 2005, IAU Circ., 8474
- Zheng, W., & Filippenko A. V., 2017, ApJ, 838, L4
- Zheng, W., Silverman, J. M., Filippenko, A. V., et al., 2013, ApJ, 778, L15

TABLE 1
 THE 9 EXTREMELY WELL-OBSERVED TYPE IA SUPERNOVAE

SN	known t_0 (MJD) ^a	filter	t_b	α_r	α_d	s	χ^2/dof
ASASSN-14lp	56998.39	<i>V</i>	23.2±0.7	1.48±0.13	2.25±0.10	1.38±0.14	109.43 / 20 = 5.47
ASASSN-14lp		<i>u</i>	25.0±0.8	2.81±0.08	5.37±0.18	0.36±0.03	350.62 / 29 = 12.09
ASASSN-14lp		<i>g</i>	33.5±1.3	1.88±0.04	4.37±0.17	0.44±0.03	366.15 / 36 = 10.17
ASASSN-14lp		<i>r</i>	25.7±1.8	1.65±0.03	2.80±0.24	0.86±0.13	301.56 / 22 = 13.70
ASASSN-14lp		<i>i</i>	15.0±0.4	1.73±0.03	1.82±0.06	1.58±0.14	156.04 / 19 = 8.21
iPTF13ebh	56607.85	<i>B</i>	18.7±0.2	1.91±0.04	3.58±0.08	1.24±0.06	49.52 / 16 = 3.09
iPTF13ebh		<i>V</i>	20.8±0.5	1.90±0.03	2.93±0.13	1.11±0.10	100.95 / 16 = 6.30
iPTF13ebh		<i>u</i>	15.8±0.3	2.53±0.11	3.90±0.16	0.94±0.11	32.83 / 13 = 2.52
iPTF13ebh		<i>g</i>	21.7±0.4	1.99±0.03	4.07±0.13	0.84±0.05	176.37 / 16 = 11.02
iPTF13ebh		<i>r</i>	14.9±0.1	1.80±0.03	1.58±0.02	3.44±0.19	94.93 / 16 = 5.93
iPTF13ebh		<i>i</i>	12.8±0.2	1.87±0.05	1.59±0.05	3.16±0.39	58.09 / 11 = 5.28
2011fe	55796.687	<i>B</i>	27.0±0.7	2.52±0.16	4.75±0.15	0.53±0.03	315.26 / 129 = 2.44
2011fe		<i>V</i>	19.5±0.1	2.18±0.04	2.33±0.02	1.40±0.04	548.44 / 126 = 4.35
2011fe		<i>R</i>	20.7±0.4	2.17±0.03	2.70±0.08	1.12±0.07	444.17 / 107 = 4.15
2011fe		<i>I</i>	15.0±0.3	2.28±0.04	2.14±0.06	1.69±0.14	475.75 / 105 = 4.53
2011fe		<i>g</i>	24.0±0.3	2.21±0.03	3.21±0.05	0.80±0.03	2892.49 / 504 = 5.73
2009ig	55062.910	<i>B</i>	30.8±3.6	1.66±0.10	4.25±0.61	0.56±0.15	83.81 / 28 = 2.99
2009ig		<i>V</i>	18.7±0.4	1.51±0.11	1.65±0.05	2.41±0.24	153.90 / 28 = 5.49
2009ig		<i>R</i>	26.9±3.7	1.68±0.05	2.99±0.47	0.74±0.20	174.66 / 24 = 7.27
2009ig		<i>I</i>	20.0±3.1	1.86±0.10	2.53±0.42	0.83±0.29	43.85 / 22 = 1.99
2013dy	56482.986	<i>B</i>	23.4±0.6	1.87±0.07	3.09±0.11	0.97±0.11	35.30 / 42 = 0.84
2013dy		<i>V</i>	19.7±0.3	1.77±0.04	1.99±0.04	1.70±0.14	44.92 / 42 = 1.06
2013dy		<i>R</i>	25.1±3.0	1.85±0.06	2.97±0.45	0.82±0.23	43.97 / 26 = 1.69
2013dy		<i>I</i>	18.5±1.8	1.85±0.10	2.35±0.32	1.15±0.35	8.88 / 23 = 0.38
2013dy		<i>U</i>	22.7±1.7	2.18±0.17	3.82±0.36	0.71±0.18	15.51 / 42 = 0.36
2012cg	56063.950	<i>B</i>	28.1±3.7	2.06±0.10	4.17±0.67	0.58±0.17	11.44 / 28 = 0.40
2012cg		<i>V</i>	20.9±0.8	1.76±0.04	2.10±0.11	1.63±0.24	20.20 / 28 = 0.72
2012cg		<i>R</i>	22.5±2.1	1.83±0.07	2.54±0.32	1.13±0.30	37.72 / 21 = 1.79
2012cg		<i>I</i>	16.4±0.9	1.85±0.08	1.95±0.16	1.66±0.39	14.67 / 19 = 0.77
KSN-2011b	995.710 ^b	broad	23.1±0.3	2.38±0.02	3.33±0.06	0.71±0.03	2185.09 / 57 = 38.33
KSN-2011c	1075.914 ^b	broad	22.7±0.4	1.77±0.05	2.63±0.12	1.97±0.23	303.76 / 60 = 5.06
KSN-2012a	1328.466 ^b	broad	22.0±0.7	2.01±0.04	3.22±0.13	0.70±0.06	1153.31 / 53 = 21.76

^a References are given in Section 2.2, and data within 3.0 days after t_0 are not included in the fitting.

^b KJD = MJD−54832.5. Its broadband filter is plotted as the *R* band.

TABLE 2
THE 56 WELL-OBSERVED TYPE IA SUPERNOVAE

SN	subtype	z	$t_{0,B}$	$t_{0,B}$ err ^a	$t_{p,B}$	$t_{r,B}$	$\Delta m_{15}(B)$	Δ
From LOSS								
1998dh	Ia-norm	0.0077	2451013.6	0.7	2451029.4	15.7	1.21	0.0015
1998dm	Ia-norm	0.0055	2451043.1	0.7	2451060.9	17.7	0.98	-0.2488
1999by	Ia-91bg	0.0027	2451296.1	0.7	2451308.5	12.4	1.95	1.5087
1999cp	Ia-norm	0.0103	2451346.3	0.7	2451363.8	17.3	1.01	-0.0837
1999dq	Ia-99aa	0.0137	2451417.8	0.8	2451436.4	18.4	0.87	-0.3112
1999gp	Ia-norm	0.0260	2451531.1	0.8	2451549.6	18.0	0.73	-0.3633
2000cx	Ia-pec	0.0070	2451738.0	0.7	2451752.3	14.2	0.94	0.2128
2000dn	Ia-norm	0.0308	2451807.7	1.4	2451824.5	16.3	1.03	-0.0058
2000dr	Ia-norm	0.0178	2451821.0	0.7	2451834.1	12.9	1.80	0.9319
2000fa	Ia-norm	0.0218	2451874.7	0.8	2451891.7	16.7	0.89	-0.1939
2001en	Ia-norm	0.0153	2452176.2	0.7	2452192.8	16.3	1.19	0.1095
2001ep	Ia-norm	0.0129	2452183.0	0.7	2452200.0	16.8	1.43	0.1458
2002bo	Ia-norm	0.0053	2452340.9	0.7	2452356.7	15.7	1.10	-0.0620
2002cr	Ia-norm	0.0103	2452391.9	0.7	2452408.7	16.6	1.21	0.0403
2002dj	Ia-norm	0.0104	2452435.0	0.7	2452450.6	15.4	1.06	0.0109
2002dl	Ia-pec	0.0152	2452439.2	0.7	2452452.5	13.0	1.85	1.0411
2002eb	Ia-norm	0.0265	2452475.8	0.7	2452494.5	18.2	0.91	-0.3094
2002er	Ia-norm	0.0090	2452508.4	0.7	2452524.5	15.9	1.24	0.1195
2002fk	Ia-norm	0.0070	2452530.0	0.7	2452548.0	17.9	1.01	-0.1163
2002ha	Ia-norm	0.0132	2452566.2	0.7	2452581.3	14.9	1.31	0.3856
2002he	Ia-norm	0.0248	2452571.6	0.8	2452585.9	13.9	1.32	0.4099
2003cg	Ia-norm	0.0053	2452713.2	1.0	2452729.4	16.1	0.93	-0.0201
2003fa	Ia-99aa	0.0391	2452788.0	0.7	2452807.3	18.5	0.86	-0.3534
2003gn	Ia-norm	0.0333	2452837.8	0.9	2452852.7	14.4	1.26	0.2899
2003gt	Ia-norm	0.0150	2452845.0	0.7	2452862.0	16.7	1.00	-0.0191
2003W	Ia-norm	0.0211	2452664.0	0.8	2452678.9	14.6	1.04	-0.1525
2003Y	Ia-91bg	0.0173	2452665.9	0.8	2452676.6	10.5	1.79	1.5668
2004at	Ia-norm	0.0240	2453075.2	0.7	2453092.1	16.6	1.02	-0.1025
2004dt	Ia-norm	0.0185	2453223.3	0.7	2453240.3	16.7	1.11	-0.1102
2004ef	Ia-norm	0.0298	2453250.0	0.7	2453264.2	13.8	1.41	0.3373
2004eo	Ia-norm	0.0148	2453262.4	0.7	2453278.5	15.8	1.37	0.2798
2005cf	Ia-norm	0.0070	2453517.7	0.7	2453533.7	15.9	1.03	-0.1080
2005de	Ia-norm	0.0149	2453581.1	0.7	2453598.8	17.4	1.18	0.0495
2005ki	Ia-norm	0.0203	2453690.0	0.7	2453705.4	15.1	1.25	0.3400
2005M	Ia-91T	0.0230	2453384.7	0.8	2453405.8	20.5	0.86	-0.4287
2006cp	Ia-norm	0.0233	2453879.6	0.8	2453897.5	17.5	1.12	-0.1903
2006gr	Ia-norm	0.0335	2453993.5	1.2	2454012.4	18.3	0.92	-0.3245
2006le	Ia-norm	0.0172	2454030.8	0.8	2454047.7	16.6	0.86	-0.2751
2006X	Ia-norm	0.0064	2453770.4	0.8	2453786.5	16.0	1.28	-0.0228
2007af	Ia-norm	0.0062	2454157.5	0.7	2454174.4	16.8	1.18	-0.0064
2007le	Ia-norm	0.0067	2454383.7	0.8	2454398.8	15.0	0.98	-0.1349
2007qe	Ia-norm	0.0244	2454412.6	0.9	2454429.0	16.0	1.01	-0.2030
2008bf	Ia-norm	0.0251	2454537.6	1.3	2454554.7	16.7	0.93	-0.1849
2008ec	Ia-norm	0.0149	2454658.2	0.7	2454674.0	15.6	1.32	0.1941
From CfA3								
2001V	Ia-norm	0.0162	51955.183	0.7	51972.446	17.0	0.67	-0.2967
2005hk	Iax	0.0118	53666.101	0.8	53684.385	18.1	1.65	-0.2331
2006ax	Ia-norm	0.0180	53808.486	0.9	53827.026	18.2	1.09	-0.1657
2006lf	Ia-norm	0.0130	54030.365	1.0	54045.385	14.8	1.32	0.3188
2007bd	Ia-norm	0.0319	54191.882	0.7	54205.783	13.5	1.03	0.2778
2007ci	Ia-norm	0.0194	54233.021	0.7	54246.246	13.0	1.91	0.8581
From CSP								
2005kc	Ia-norm	0.0137	3679.7901	0.7	3697.4031	17.4	1.19	0.0055
2005ke	Ia-91bg	0.0045	3684.9211	0.7	3698.2680	13.3	1.77	1.6190
2007on	Ia-norm	0.0062	4404.8806	0.7	4419.7535	14.8	1.87	0.9558
2008bc	Ia-norm	0.0157	4532.0783	0.7	4549.1804	16.8	0.87	-0.2790
2008gp	Ia-norm	0.0328	4760.8915	0.7	4779.0086	17.5	1.05	-0.0576
2008hv	Ia-norm	0.0125	4801.8928	0.7	4816.5393	14.5	1.22	0.2761

^a include the 0.7 days systematic error estimated from the fitting method